frontiers in Materials

ORIGINAL RESEARCH
published: 02 November 2021
doi: 10.3389/fmats.2021.776817

Synthesis and Photocatalytic Degradation of Water to Produce Hydrogen from Novel Cerium Dioxide and Silver-Doped Cerium Dioxide Fiber Membranes by the Electrospinning Method

Xingyu Pu[1,2], *Chencheng Wang*[1], *Xingwang Chen*[1], *Jing Jin*[1], *Wanfei Li*[1] *and Feng Chen*[1,2]*

[1]School of Materials Science and Engineering, Suzhou University of Science and Technology, Suzhou, China, [2]Tianping Collage of Suzhou University of Science and Technology, Suzhou, China

OPEN ACCESS

Edited by:
Hua Yang,
Lanzhou University of Technology, China

Reviewed by:
Fang Leiming,
China Academy of Engineering Physics, China
Guangzhuang Sun,
Chongqing Three Gorges University, China

***Correspondence:**
Feng Chen
ujschenfeng@163.com

Specialty section:
This article was submitted to Semiconducting Materials and Devices, a section of the journal Frontiers in Materials

Received: 14 September 2021
Accepted: 20 September 2021
Published: 02 November 2021

Citation:
Pu X, Wang C, Chen X, Jin J, Li W and Chen F (2021) Synthesis and Photocatalytic Degradation of Water to Produce Hydrogen from Novel Cerium Dioxide and Silver-Doped Cerium Dioxide Fiber Membranes by the Electrospinning Method. Front. Mater. 8:776817. doi: 10.3389/fmats.2021.776817

The sol-gel method combined with the electrospinning technique were used to synthesize CeO_2 nanofiber membranes and CeO_2 fiber membranes doped with different contents of nano-silver. The thermal degradation behavior, phase structure, morphology, and optical and photocatalytic hydrogen production efficiency of CeO_2 nanofiber membranes and CeO_2 fiber membranes doped with different contents of nano-silver were studied. X-ray diffraction (XRD) results indicate that the increase of silver concentration can inhibit the formation of CeO_2 crystal. Scanning electron microscopy (SEM) and transmission electron microscopy (TEM) observations show that in the prepared CeO_2 with a diameter of about 100 nm and fiber membrane material doped with nano-silver, the fiber is made of a large number of accumulating grains. Analysis of optical properties found that the doped nano–silver CeO_2 fiber membranes enhance the absorption of visible light and reduce the band gap of the material. Photocatalytic experiments show that the cerium dioxide nanofibers doped with nano-silver can greatly improve the photocatalytic performance of materials than that of pure CeO_2. The Ag/CeO_2 fiber membrane with the Ag/CeO_2 molar ratio of 3:50 possesses the highest photocatalytic hydrogen production efficiency because of its high electron hole transfer and separation efficiency. This novel synthesis strategy can be used to prepare other broad band gap semiconductor oxides and enhance their photocatalytic activity.

Keywords: photocatalytic degradation of water, cerium dioxide, silver, fiber membranes, electrospinning

INTRODUCTION

With the rapid development of the global economy, the demand for energy continues to grow, while the concern of greenhouse gas and aerosol emissions is increasing, the development of clean, renewable new energy has become the most urgent task for countries all over the world (Chen et al., 2020). As a secondary energy source, hydrogen energy has the advantages of being abundant, economical, clean, efficient, storable, and transportable, and is generally regarded as one of the most ideal pollution-free green energy sources in the 21st century (Prekob et al., 2020). At present, one of

the main means of hydrogen production is photocatalytic decomposition of water to produce hydrogen, and the key of this is to choose a good photocatalyst (Bashiri et al., 2020; Abd-Rabboh et al., 2021; Hamdy et al., 2021). Therefore, it is interesting to develop new photocatalysts to construct specific defect structures and to study their photocatalytic activity.

As the one of the most abundant rare elements in nature, cerium has a unique 4f electronic structure which makes its compounds widely used in optical, electrical, and magnetic fields (Rajesh et al., 2020; Abd-Rabboh et al., 2021; Wang et al., 2021a; Wang et al., 2021b; Syed et al., 2021). Cerium dioxide is a promising semiconductor photocatalyst, because it has the properties of n–type semiconductors such as good light–resistant corrosivity and excellent storage and release of oxygen, and its unique Ce^{3+}/Ce^{4+} valence activity makes it highly oxidative and gives it a reducing ability (Mishra et al., 2018; Wen et al., 2018; Xing et al., 2020; Wang et al., 2021c; Wang et al., 2021d). Nano–cerium dioxide possesses more special properties and applications than cerium dioxide, so researchers have more stringent requirements about morphology, size, and others (Gao et al., 2018; Gong et al., 2019; Li et al., 2021). However, research on cerium dioxide nanofibers is relatively rare. Generally, the single component CeO_2 photocatalyst has a large band gap and is difficult to respond to visible light, which greatly limits its application in the field of photocatalytic decomposition of water to produce hydrogen (Li et al., 2021). Up to now, there are three methods to improve the photocatalytic activity of CeO_2 photocatalysts (Gao et al., 2018; Malyukin et al., 2018; Mohammadiyan et al., 2018; Wen et al., 2018; Xing et al., 2020; Wang et al., 2021d; Mikheeva et al., 2021): 1) using special preparation methods to synthesize CeO_2 photocatalysts with special defect structures, 2) combining other metal oxides with a small band gap value to construct special heterojunction structure composites to enhance their light response ability, and 3) a CeO_2 photocatalyst was modified by noble metal particles to enhance the charge transfer and migration ability of the system, thus improving the photocatalytic activity of CeO_2. Noble metal particles-doped cerium dioxide is expected to show excellent physical and chemical properties (Mikheeva et al., 2021). Therefore, the preparation of cerium dioxide and noble metal particles-doped cerium dioxide by special technology and the study of their photocatalytic decomposition of water to produce hydrogen has important research significance.

In this paper, cerium dioxide composite fiber membranes and CeO_2 fiber membranes doped with different contents of nano-silver were prepared by the sol-gel method combined with electrospinning technology. The thermal decomposition behavior, phase structure, morphology, and optical and photocatalytic decomposition of water to produce hydrogen of cerium dioxide composite fiber membranes and CeO_2 fiber membranes doped with different contents of nano-silver were studied by various characterization methods. Based on the energy band theory and photocatalytic experiment results, a photocatalytic mechanism is proposed.

MATERIALS AND METHODS

Materials

All reagents were analytical grade and were used without further treatment. Hexahydrate nitrate and polyvinylpyrrolidone (PVP) were purchased from Aladdin Reagent (China) Co., Ltd. Anhydrous ethanol, silver nitrate, and acetic acid were purchased from Sinopharm Group Chemical Reagent Co., Ltd.

Preparation of Cerium Dioxide Fiber Membranes

A total of 3 g of polyvinylpyrrolidone (PVP) was weighed and added to 50 ml of ethanol, then the mixture, known as solution A, was stirred for 3 h until completely dissolved. In total, 2.171 g of cerium nitrate hexahydrate was dissolved in 10 ml of ethanol. After stirring, the solution was slowly added dropwise to solution A and stirred for about 6 h. The solution was spray–coated by the electrospinning method with a temperature of 20°C and a relative humidity of 50%. The film was dried in a vacuum oven at 40°C for 12 h. The dried film was then calcined in a muffle furnace at 550°C and incubated for 0.5 h. And finally a pale yellow cerium dioxide film was obtained.

Preparation of Cerium Dioxide Fiber Membrane Doped With Nano-Silver

Solution A and the cerium source solution were prepared under the same conditions and the two solutions were mixed under stirring. A total of 0.017 g of $AgNO_3$ was added to 5 ml of deionized water and stirred for 20 min. The silver source solution was slowly added dropwise to the above mixed solution and stirred for 2 h. In addition, by changing the content of $AgNO_3$ in the spinning solution, the morphological characteristics and properties of the spinning film under different silver contents were investigated. The solution of 0.051 and 0.085 g of silver nitrate was prepared by the same method, which means that the molar ratios of $AgNO_3$/Ce $(NO_3)_3$ in the spinning solution were 1:50, 3:50, and 5:50. The film was prepared by an electrospinning method. After drying under the same conditions, the film was calcined in a muffle furnace to 600°C for 1 h. Finally, cerium dioxide nanofiber membranes doped with nano-silver were obtained.

Materials Characterization

The products were characterized by thermogravimetric analysis (TG) and differential scanning calorimetry (DSC). The heating rate, the air flow rate, the injection volume, and the temperature range were 20 K/min, 100 ml/min, 2 mg and 25–800°C, respectively. The composition of membranes was characterized by a Brook D8 Advance X-Ray diffractometer with a scanning angle of 20–80°, a scanning step length of 0.02°, and using Cu target Kα (λ = 0.154056 nm) radiation with a working voltage of 40 kV and a current of 40 mA. The microstructures of membranes were observed by scanning electron microscopy, while the fibers and particles constituting membranes were

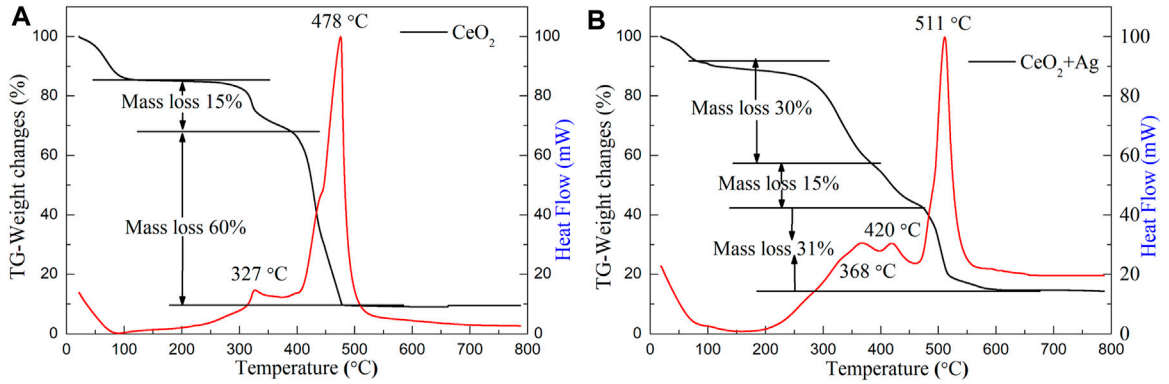

FIGURE 1 | Thermogravimetric analysis of **(A)** PVP/Ce $(NO_3)_3$ and **(B)** PVP/Ce $(NO_3)_3$/$AgNO_3$ composite fiber membranes with the Ag/CeO_2 molar ratios of 3:50 prepared by the electrospinning method.

characterized by scanning electron microscopy (SEM) and transmission electron microscopy (TEM). UV-visible absorption spectra of prepared samples were measured by an ultraviolet and visible spectrophotometer.

Photocatalytic Experiments

In order to investigate the photocatalytic properties of the prepared cerium dioxide fiber membranes and the cerium dioxide fibers doped with different proportions of nano-silver, they were applied to the reaction of photocatalytic degradation of water to produce hydrogen and compared with the bulk pure cerium oxide. The Labsolar H_2 photolysis system was developed by Beijing Prefectlight Technology Co., Ltd., and the detection device was a Shanghai Tianmei GC7900 Gas Chromatograph, with a Microsolar300 high performance analog daylight xenon lamp used as the simulation light source. A 100-mg sample was added to 100 ml of deionized water, and sodium sulfite was added as the sacrificial agent to carry out photocatalytic hydrogen production. The hydrogen production of each material was compared after 6 h of illumination.

RESULTS AND DISCUSSION

Thermogravimetric Analysis-Differential Scanning Calorimetry Analysis

Figure 1A shows the TG-DSC curves of PVP/Ce $(NO_3)_3$ composite membranes prepared by the electrospinning method. It can be seen from the figure that the sample has a large weight loss process at room temperature to 100°C, and the weight loss process is the elimination of the moisture absorbed by the sample and the possible residual solvent (Wang et al., 2013). It can be also proved that membranes have certain water absorption capacities. After that there are two large weight loss processes which correspond to two distinct exothermic peaks, especially the second exothermic peak. The first exothermic peak appears at 327°C, which indicates that from 100 to 400°C, the sample first absorbs heat, and the outer layer of the composite fiber PVP begins to decompose, then the cerium nitrate in the fiber is decomposed into cerium dioxide; the weight loss of the system during this decomposition is 15% (Mohammadiyan et al., 2018). After 550°C, the reaction is basically completed, the sample weight and heat flow curve are stable, and the final quality is about 10% of the original quality. Thus, the calcination temperature of the PVP/Ce $(NO_3)_3$ composite film can be set at 550°C.

Figure 1B shows the TG-DSC analysis of PVP/Ce$(NO_3)_3$/$AgNO_3$ for composite membrane materials. It can be seen from the figure that the final mass of the sample is about 14% of the original mass throughout the reaction. The weight loss phase from room temperature to 100°C is the residual solvent and moisture contained in the sample. There are three exothermic peaks since then, with two adjacent exothermic peaks from 100 to 450°C, then the process undergoes a more complex reaction. As can be seen from **Figure 1B**, the exothermic peak at 368°C corresponds to the initial decomposition of the polymer template, then cerium nitrate decomposes and oxidizes to cerium oxide. and the weight loss is about 30%. The exothermic peak at 420°C is a sign that the silver nitrate is thermally decomposed into silver nanoparticles with a weight loss ratio of 15%. The complete decomposition of PVP occurs between 450 and 600°C. From the TG-DSC curve, it can be seen that the thermal decomposition has been basically completed at 600°C. After the sample stabilizes, the heat flow curve tends to be smooth. The calcination temperature of the PVP/Ce $(NO_3)_3$/$AgNO_3$ composite film can be set at 600°C. When silver nitrate is introduced, a higher sintering temperature is needed to obtain the target product.

X-Ray Diffraction Analysis

Figure 2A shows the XRD pattern of PVP/Ce$(NO_3)_3$ composite fiber membranes and the membranes after calcination at 550°C in air and incubated for 0.5 h. The result indicates that the membranes after calcination have obvious diffraction peaks at $2\theta = 28.4°$, 33.0°, 47.4°, 56.1°, 59.0°, 69.2°, 76.4°, and 78.8°, corresponding to the (111), (200), (220), (311), (222), (400), (331), and (420) crystal faces of cubic fluorite crystal CeO_2, which is consistent with the standard

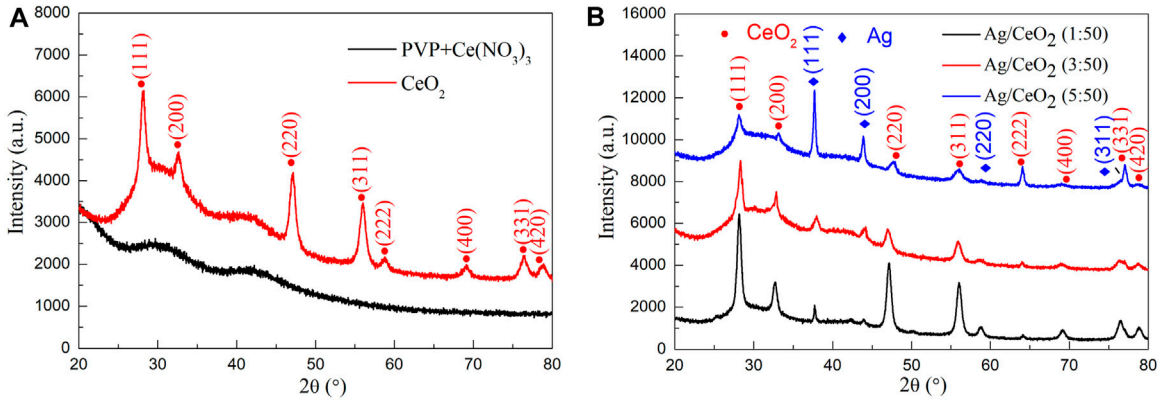

FIGURE 2 | (A) XRD pattern of PVP/Ce $(NO_3)_3$ composite fiber membrane and CeO_2 nanofiber membrane calcined at 550°C. **(B)** XRD pattern of the cerium oxide fiber doped with nano-silver with the Ce $(NO_3)_3/AgNO_3$ molar ratios of 1:50, 3:50, and 5: 50.

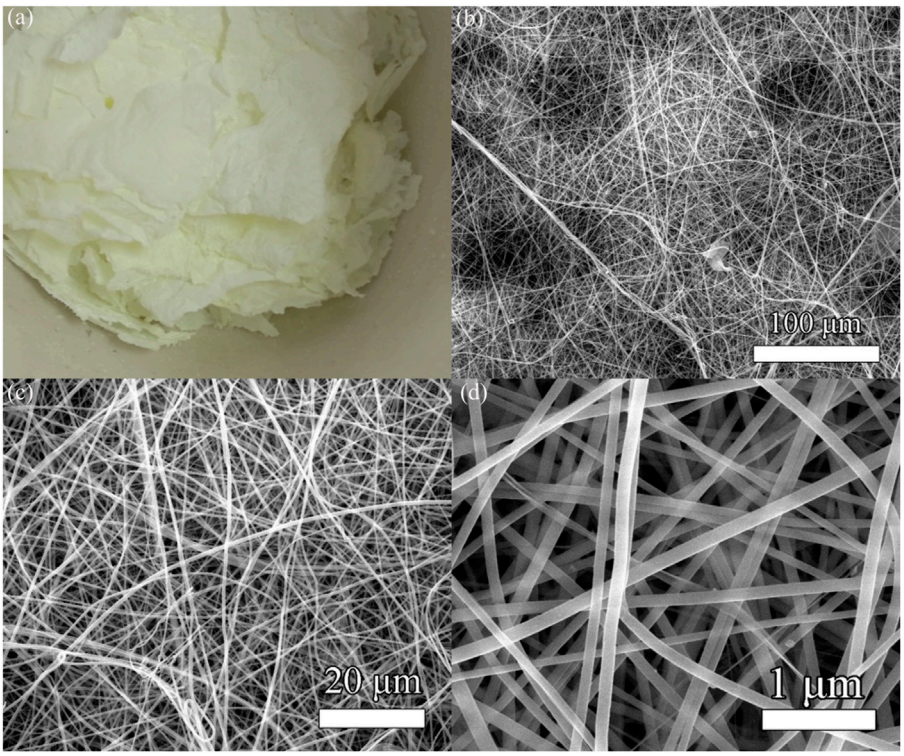

FIGURE 3 | (A) Real photographs of CeO_2 nanofiber membranes. **(B–D)** SEM images of CeO_2 nanofiber membranes at different magnifications.

card of cerium dioxide (JCPDS card no. 43 -1002). Because the fibers in membranes are covered and encapsulated by a large number of polymer PVPs, two amorphous bread peaks appear in the XRD pattern which are the diffraction peaks of the polymer. In addition, there were no other sharp diffraction peaks, and it was found that the composite fiber membrane synthesized by the electrospinning method was formed into a face-centered cubic cerium dioxide with standard card JCPDS card no. 21-1272 after calcination.

Figure 2B shows the XRD pattern of PVP/Ce $(NO_3)_3/AgNO_3$ composite fiber membranes with different silver content after calcination at 600°C for 1 h in muffle furnace, which contains the molar ratios of $AgNO_3$/Ce $(NO_3)_3$ of 1:50, 3:50, and 5:50 respectively. From the XRD curve, it can be seen that at 2θ = 28.4°, 33.0°, 47.4°, 56.1°, 59.0°, 69.2°, 76.4°, and 78.8°, the diffraction peaks correspond to (111), (200), (220), (311), (222), (400), (331), and (420) planes of the cubic fluorite crystal CeO_2. At diffraction angles of 2θ = 37.98°, 44.18°, 64.42°, and 77.26°, the diffraction

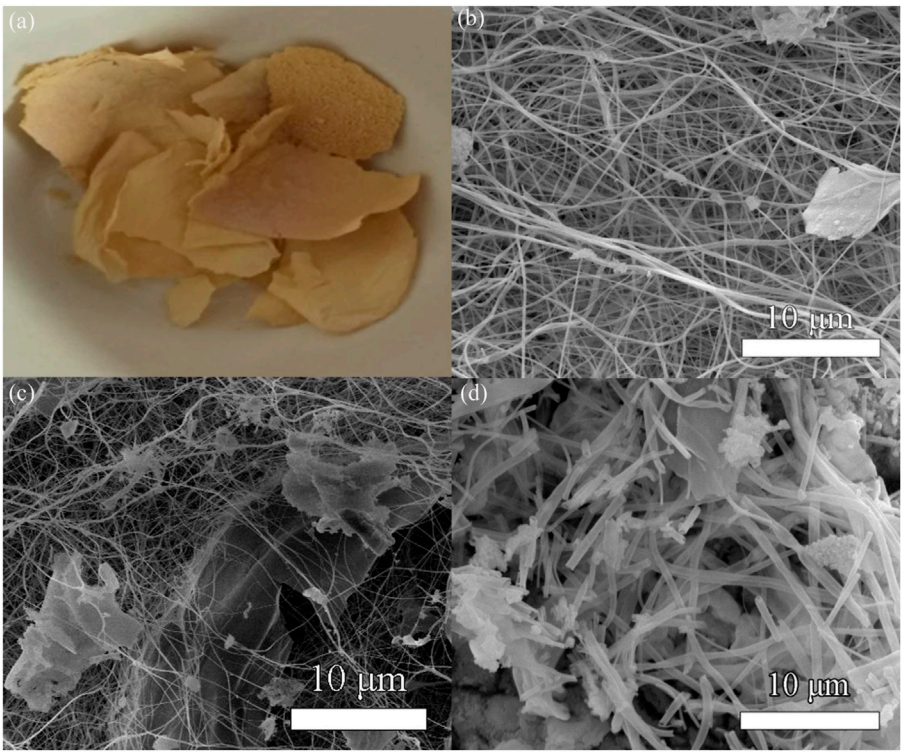

FIGURE 4 | (A) Real photographs of Ag/CeO_2 fiber membranes. SEM images of the cerium oxide fiber doped with nano-silver with the Ag/CeO_2 molar ratios of **(B)** 1:50, **(C)** 3:50, and **(D)** 5: 50.

signals correspond to the (111), (200), (220), and (311) planes of silver, which match the standard card of the nano-silver cubic crystal structure (JCPDS card no. 04-0783). All the diffraction peaks for the three samples are cerium dioxide and nano-silver. And with the increase of the relative content of silver, the peak of nano-silver shows more strongly, while the diffraction peak of cerium dioxide is weakened. All of these have proven that the prepared material is a thin cerium dioxide fiber film material loaded with nano-silver.

Scanning Electron Microscopy Analysis

Figure 3 shows the real photographs and SEM images of the PVP/$Ce(NO_3)_3$ composite fiber membranes and the membranes after calcination at 550°C in air. **Figure 3A** shows the real photographs of cerium dioxide after calcination. Obviously, the membrane has a greater degree of contraction and is pale yellow, the weight is very light and fragile, but still retains the structure of lamellae. **Figure 3B** shows the SEM image at a magnification of 100 μm, which shows that the sample is relatively flat and compact and has a high porosity. **Figure 3C** shows the SEM image at a magnification of 20 μm. It can be seen that the sample consists of a large number of nanofibers, and the fibers are disordered, within layers, and with no accumulation of fibers. **Figure 3D** shows the high resolution FESEM picture, the scale is 1 μm, the fiber is straight, the thickness and the distribution are uniform, the fiber diameter is about 100 nm, and has a very high aspect ratio.

Figure 4 shows the real photographs and SEM images of the Ag/CeO_2 fiber membrane prepared at different molar ratios of $Ce(NO_3)_3/AgNO_3$ including 1:50, 3:50, and 5:50. **Figure 4A** shows the real photographs of the sample after calcination at 600°C. It can be seen that the sample still retains the morphology of the membranes, and the addition of silver ions significantly increases the color of the sample which presents as brownish yellow when compared to the CeO_2 fiber membrane. **Figures 4B–D** show the SEM images of the Ag/CeO_2 fiber membrane prepared at different molar ratios of $Ce(NO_3)_3/AgNO_3$ including 1:50, 3:50, and 5:50. It can be seen that the sample still retains the fiber morphology. The fiber thickness of the Ag/CeO_2 membranes loaded with nano-silver is relatively uneven and the fiber distribution is more cluttered compared with the pure cerium oxide fiber. There is a phenomenon of heap and fracture in the microstructure of the membranes. Because of the introduction of metallic silver ions in the spinning solution, the introduction of this inorganic salt changes the electrostatic parameters of the spinning solution, making the electrospinning process of the spinning fluid become more complex and changeable and making fibers of uneven thickness. With the increase of silver ions, the overall morphology of the fiber becomes more uneven, and agglomeration is becoming more and more serious.

Transmission Electron Microscopy Analysis

Figure 5 shows the TEM and HRTEM images of the nano-cerium dioxide membrane material. From **Figure 5A**, it can be observed that the cerium dioxide is a fibrous structure and the diameter of

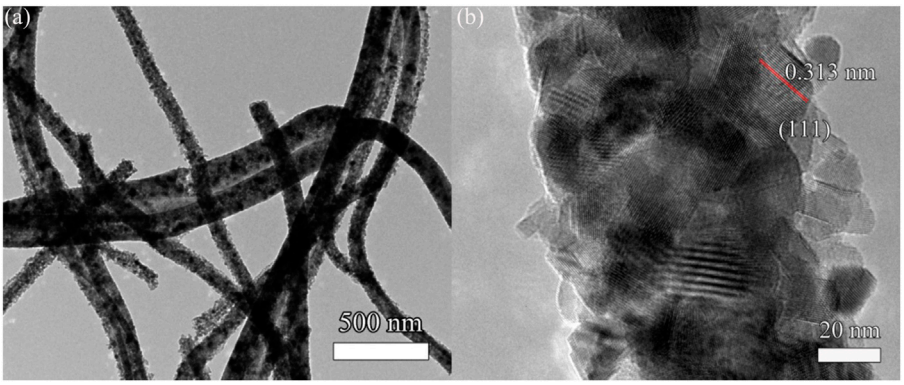

FIGURE 5 | (A) TEM image and **(B)** high-resolution transmission electron microscopy (HRTEM) of cerium dioxide fiber membranes.

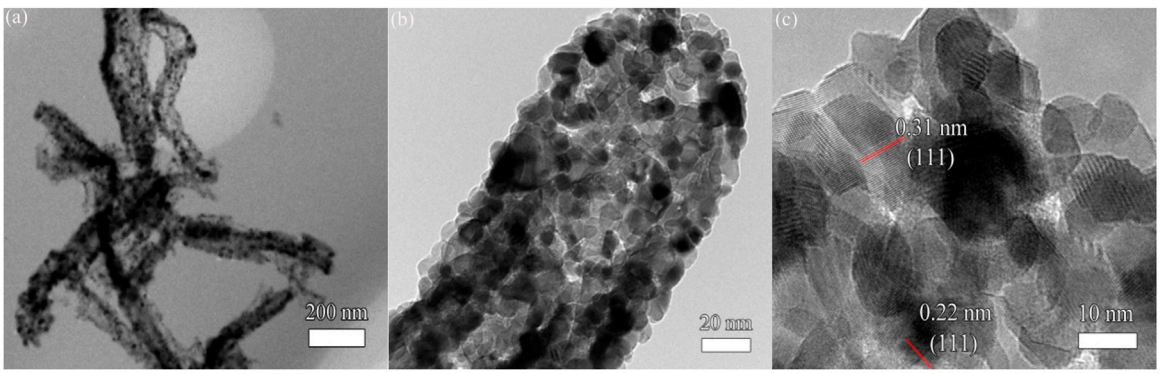

FIGURE 6 | (A) TEM image, **(B)** enlarged TEM image, and **(C)** HRTEM image of Ag/CeO_2 fiber membrane with an Ag/CeO_2 molar ratio of 3:50.

the fiber is about 100 nm. The morphology is well preserved and has a large aspect ratio. **Figure 5B** shows the high–resolution transmission electron microscopy (HRTEM) image. It can be seen that the fiber is actually made of nano–sized cerium dioxide grains. The cerium dioxide grains forming the fibers have a grain size of 15 nm, and there is a large number of lattice lines of cerium dioxide crystals. By measuring the interplanar spacing, it can be seen that the exposed active surface is a (111) plane and $d_{(111)}$ = 0.313 nm.

Figure 6 shows the TEM and HRTEM images of the Ag/CeO_2 fiber membrane with an Ag/CeO_2 molar ratio of 3:50. **Figure 6A** shows the TEM image of the sample at a 200-nm scale. It can be seen from the figure that the fibrous Ag/CeO_2 has a diameter of about 100 nm. **Figure 6B** shows an enlarged TEM image at 20 nm, and it can be clearly seen that the fibers are deposited from a large number of crystal particles with a grain size of about 10 nm. **Figure 6C** shows the HRTEM image, at 10 nm, of the Ag/CeO_2 fiber membrane with the Ag/CeO_2 molar ratio of 3:50. A large number of lattice lines are shown in which the spacing of most of the lattice lines is 0.31 nm corresponding to the (111) plane of the cerium dioxide cubic crystal structure, and there is also a lattice line with a crystal plane spacing of 0.22 nm corresponding to the (111) crystal face of Ag nanoparticles. All of the above analyses prove that the material is cerium dioxide fiber material doped with nano-silver, which corresponds to the XRD result.

Optical Properties

Figure 7 shows the UV-Vis absorption spectra and its corresponding forbidden band width calculation for the pure cerium oxide fiber membrane and the cerium oxide fiber membrane with different amounts of loaded silver. As can be seen from **Figure 7A**, the light absorption of the pure cerium dioxide fiber membrane in the wavelength range of 400–800 nm is weak, and gradually increases before 400 nm. While compared with the nano–silver-loaded material, the absorption of nano-silver-loaded material in the visible light area has significantly improved. This is because the nano–silver loaded in the CeO_2 semiconductor brings defects, resulting in changes in the band structure and reduction of the band gap width. And the nano-silver particles have the capability to absorb light, so the

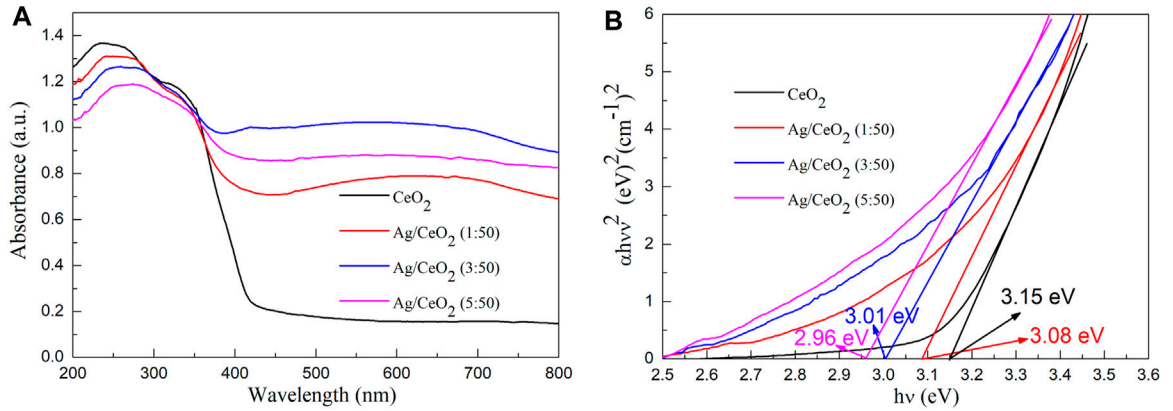

FIGURE 7 | (A) UV-Vis diffuse scattering spectra of pure cerium dioxide nanofiber membranes and cerium dioxide nanofiber membranes doped with different amounts of nano-silver. **(B)** The optical band gap (Eg) values of pure cerium dioxide nanofiber membranes and cerium dioxide nanofiber membranes doped with different amounts of nano-silver.

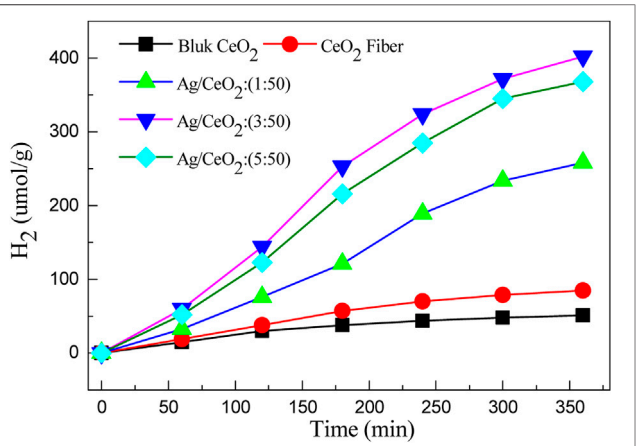

FIGURE 8 | Hydrogen evolution of different materials under visible light irradiation.

material on the absorption of visible light intensity is significantly enhanced.

The band gap energy (Eg) values of pure cerium dioxide nanofiber membranes and cerium dioxide nanofiber membranes doped with different amounts of nano-silver were obtained by absorbance spectra using the Tauc relation (Tang et al., 2020; Wang et al., 2020; Wang and Tian, 2020; Wang et al., 2021e; Gao et al., 2021).

$$(F(R)h\nu)^n = A\left(h\nu - E_g\right) \quad (1)$$

Where ν is the frequency, A is the absorption coefficient, and n is equal to 2. The band gap of the samples are obtained by a simple intercept method. In **Figure 7B**, the band gap width of pure cerium oxide fibers is consistent with the literature (Gao et al., 2018) (3.15 eV). When the molar ratios of Ag/CeO_2 are 1:50, 3:50, and 5:50, the corresponding band gap values are 3.08, 3.01, and 2.96 eV, respectively. It can be seen that the band gap of the Ag/CeO_2 fiber membrane decreases gradually with the increase of the relative content of metallic silver. After modification of the CeO_2 fiber membrane by Ag nanoparticles, the band gap of the CeO_2 fiber membrane is reduced.

Photocatalytic Decomposition of Water to Produce Hydrogen

Figure 8 shows the hydrogen production of bulk cerium dioxide, cerium dioxide nanofibers, and three different silver-doped cerium dioxide nanofiber membranes. It can be seen from the figure that the hydrogen production of the sample is increasing with the progress of the reaction, but the efficiency of hydrogen production decreases with the consumption of the sacrificial agent and the decrease of the catalyst activity. The hydrogenation efficiency of bulk cerium dioxide and cerium dioxide nanofibers are very low because the cerium dioxide only absorbs ultraviolet light, which leads to low photocatalytic activity. The photocatalytic hydrogen production efficiency of the noble metal nano-silver-doped cerium dioxide fiber material has been greatly improved due to the nano-silver as it is in contact with the cerium dioxide crystal to form a heterojunction, and the band of the semiconductor is bent at the interface. Then, the electrons shift from a high Fermi level to a low Fermi level, forming a Schottky barrier in the materials. Comparing 3 M ratios of Ag/CeO_2, the photocatalytic hydrogen is the highest when the molar ratio of Ag/CeO_2 is 3:50, and the hydrogen production is about 402 μmol/g after 6 h of illumination. The photocatalytic activity of CeO_2 fiber increases with the addition of nano-silver, but the photocatalytic activity decreases when the doped noble metal nano-silver goes over a certain limit. This is because the excess of nano-silver particles will become the recombination center of the carrier, which will capture the hole on the surface of the CeO_2 fiber, leading to a decrease of photogenerated carrier density and

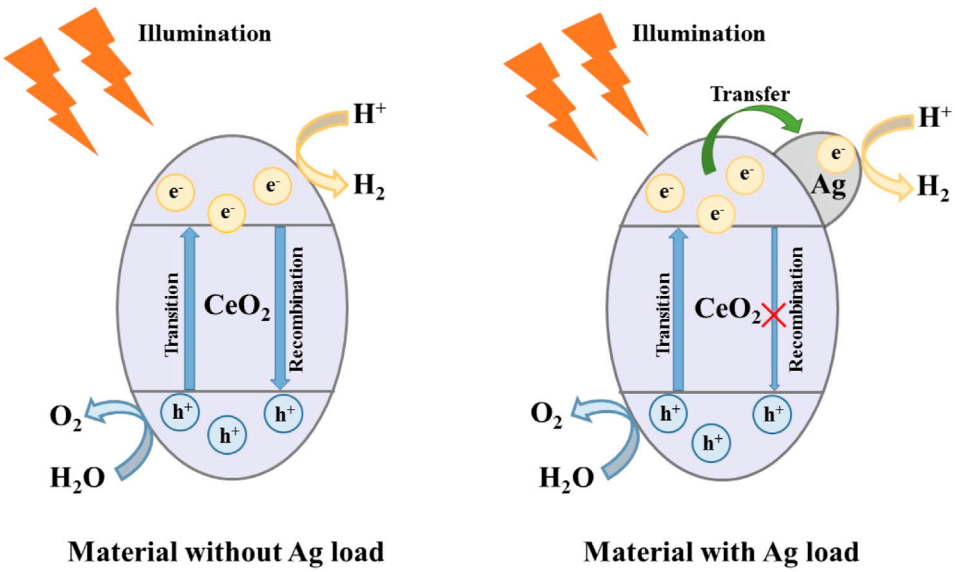

FIGURE 9 | Photocatalytic mechanism of CeO_2 and Ag/CeO_2 photocatalysts.

a reduction in photocatalytic performance. While too much precious metal particles will cover the active center of CeO_2, which will also reduce the photocatalytic performance of the system. Moreover, it can be seen from the SEM image that CeO_2 has a tendency to accumulate into blocks as the amount of silver increases which can make the specific surface area reduce.

Photocatalytic Mechanism

Based on band theory and experimental results, **Figure 9** shows the photocatalytic mechanism of CeO_2 and Ag/CeO_2 photocatalysts. When visible light irradiates on the surface of CeO_2, because the band gap of CeO_2 is large, it can only respond to ultraviolet light, so the probability of valence band electron transition to the conduction band is small. At the same time, the photocatalytic hydrogen production efficiency is low because a small number of electrons in the conduction band are easily recombined with the holes in the valence band. When Ag is loaded on the surface of CeO_2, the electron transition from the valence band of CeO_2 to its conduction band is accelerated, so that the Ag/CeO_2 photocatalyst can respond to visible light. The electrons that transition to the CeO_2 conduction band will accelerate the transfer to Ag particles, preventing the electron from recombination with the holes of the CeO_2 conduction band. The transfer and separation of electrons and holes play an important role in the whole process of photocatalytic hydrogen production. Ag particles act as the carrier of charge carrier transfer during the whole process.

CONCLUSION

CeO_2 nanofiber membranes and CeO_2 fiber membranes doped with different contents of nano-silver were prepared by the sol-gel method and electrospinning technique. The CeO_2 and Ag/CeO_2 nanofiber membranes were characterized by TG-DSC, XRD, SEM, TEM, and UV-Vis, and their photocatalytic activity was investigated by the photocatalytic decomposition of water. The electrospinning method successfully prepared CeO_2 with a diameter of about 100 nm and fiber membrane materials doped with nano-silver; the fiber is made of a large number of accumulated grains. The increase of silver concentration can inhibit formation of CeO_2 crystal. With the increase of the relative content of silver ions, the difficulty of spinning increases, the morphology of the fibers becomes more and more cluttered, and the accumulation phenomenon becomes more and more serious. The doped nano–silver CeO_2 fiber membrane enhances the absorption of visible light and reduces the band gap of the material, so its photocatalytic performance is significantly improved. In the photocatalytic hydrogen production, the cerium dioxide nanofibers doped with nano-silver can greatly improve the photocatalytic performance of materials. The Ag/CeO_2 fiber membrane with the Ag/CeO_2 molar ratio of 3:50 exhibits the highest photocatalytic hydrogen production efficiency, and the hydrogen production after irradiation for 6 h is about 402 μmol/g due to its high electron hole transfer and separation efficiency.

DATA AVAILABILITY STATEMENT

The original contributions presented in the study are included in the article/Supplementary Material, further inquiries can be directed to the corresponding authors.

AUTHOR CONTRIBUTIONS

XP was responsible for synthesis experiments, performance tests and data analysis. CW and XC were responsible for material characterization. JJ was responsible for the analysis and guidance of XRD and UV tests. WL is responsible for analyzing the reaction mechanism. FC was responsible for experimental design and paper revision.

FUNDING

This work was supported by National Natural Science Foundation of China (21773291); Natural Science Foundation of Jiangsu Province (BK20180103); Qing Lan Project of Jiangsu Province; Suzhou Key Laboratory for Nanophotonic and Nanoelectronic Materials and Its Devices.

REFERENCES

Abd-Rabboh, H. S. M., Benaissa, M., Hamdy, M. S., Ahmed, M. A., and Glal, M. (2021). Synthesis of an Efficient, and Recyclable Mesoporous BiVO4/TiO2 Direct Z-Scheme Heterojunction by Sonochemical Route for Photocatalytic Hydrogen Production and Photodegradation of Rhodamine B Dye in the Visible Region. *Opt. Mater.* 114, 110761. doi:10.1016/j.optmat.2020.110761

Bashiri, R., Mohamed, N. M., Sufian, S., and Kait, C. F. (2020). Improved Photoelectrochemical Hydrogen Production over Decorated Titania with Copper and Nickel Oxides by Optimizing the Photoanode and Reaction Characteristics. *Mater. Today Chem.* 16, 100241. doi:10.1016/j.mtchem.2020.100241

Chen, S., Skordos, A., and Thakur, V. K. (2020). Functional Nanocomposites for Energy Storage: Chemistry and New Horizons. *Mater. Today Chem.* 17, 100304. doi:10.1016/j.mtchem.2020.100304

Gao, H., Wang, Y., Gao, Q., Pan, X., Wang, S., Yang, H., et al. (2021). Phase Evolution and Photoluminescence Behavior of MMoO4 (M = Mg, Ca, Sr) Phosphors. *Optik* 241, 167040. doi:10.1016/j.ijleo.2021.167040

Gao, H., Yang, H., Yang, G., and Wang, S. (2018). Effects of Oxygen Vacancy and Sintering Temperature on the Photoluminescence Properties and Photocatalytic Activity of CeO2 Nanoparticles with High Uniformity. *Mater. Technol.* 33, 321–332. doi:10.1080/10667857.2018.1438222

Gong, X., Gao, X., Du, W., Zhang, H., Zhang, S., Nguyen, T. T., et al. (2019). Wood Powder-Derived Quantum Dots for CeO2 Photocatalytic and Anti-counterfeit Applications. *Opt. Mater.* 96, 109302. doi:10.1016/j.optmat.2019.109302

Hamdy, M. S., Abd-Rabboh, H. S. M., Benaissa, M., Al-Metwaly, M. G., Galal, A. H., and Ahmed, M. A. (2021). Fabrication of Novel polyaniline/ZnO Heterojunction for Exceptional Photocatalytic Hydrogen Production and Degradation of Fluorescein Dye through Direct Z-Scheme Mechanism. *Opt. Mater.* 117, 111198. doi:10.1016/j.optmat.2021.111198

Li, J., Wang, S., Sun, G., Gao, H., Yu, X., Tang, S., et al. (2021). Facile Preparation of MgAl2O4/CeO2/Mn3O4 Heterojunction Photocatalyst and Enhanced Photocatalytic Activity. *Mater. Today Chem.* 19, 100390. doi:10.1016/j.mtchem.2020.100390

Malyukin, Y., Seminko, V., Maksimchuk, P., Okrushko, E., Sedyh, O., and Zorenko, Y. (2018). Hydrogen Peroxide Sensing Using Ce3+ Luminescence of Cerium Oxide (CeO2-X) Nanoparticles. *Opt. Mater.* 85, 303–307. doi:10.1016/j.optmat.2018.08.063

Mikheeva, N. N., Zaikovskii, V. I., Larichev, Y. V., and Mamontov, G. V. (2021). Toluene Abatement on Ag-CeO2/SBA-15 Catalysts: Synergistic Effect of Silver and Ceria. *Mater. Today Chem.* 21, 100530. doi:10.1016/j.mtchem.2021.100530

Mishra, S., Soren, S., Debnath, A. K., Aswal, D. K., Das, N., and Parhi, P. (2018). Rapid Microwave - Hydrothermal Synthesis of CeO2 Nanoparticles for Simultaneous Adsorption/photodegradation of Organic Dyes under Visible Light. *Optik* 169, 125–136. doi:10.1016/j.ijleo.2018.05.045

Mohammadiyan, E., Ghafuri, H., and Kakanejadifard, A. (2018). Synthesis and Characterization of a Magnetic Fe3O4@CeO2 Nanocomposite Decorated with Ag Nanoparticle and Investigation of Synergistic Effects of Ag on Photocatalytic Activity. *Optik* 166, 39–48. doi:10.1016/j.ijleo.2018.03.044

Prekob, Á., Hajdu, V., Muránszky, G., Fiser, B., Sycheva, A., Ferenczi, T., et al. (2020). Application of Carbonized Cellulose-Based Catalyst in Nitrobenzene Hydrogenation. *Mater. Today Chem.* 17, 100337. doi:10.1016/j.mtchem.2020.100337

Rajesh, K., Sakthivel, P., Santhanam, A., and Venugobal, J. (2020). Incorporation of Silver Ion on Structural and Optical Characteristics of CeO2 Nanoparticles: White LED Applications. *Optik* 216, 164800. doi:10.1016/j.ijleo.2020.164800

Syed, A., Elgorban, A. M., and Al Kheraif, A. A. (2021). High Performance Nanohybrid CeO2@2D CdO Plates with Suppressed Charge Recombination: Insights of Photoluminescence, Visible-Light Photocatalysis, Intrinsic Mechanism and Antibacterial Activity. *Opt. Mater.* 121, 111510. doi:10.1016/j.optmat.2021.111510

Tang, S., Wang, S., Yu, X., Gao, H., Niu, X., Wang, Y., et al. (2020). Gamma-Ray Irradiation Assisted Polyacrylamide Gel Synthesis of Scheelite Type BaWO 4 Phosphors and its Colorimetric, Optical and Photoluminescence Properties. *ChemBioChem* 5, 10599–10606. doi:10.1002/slct.202002429

Wang, S.-F., Zhang, C., Sun, G., Chen, B., Xiang, X., Wang, H., et al. (2013). Fabrication of a Novel Light Emission Material AlFeO3 by a Modified Polyacrylamide Gel Route and Characterization of the Material. *Opt. Mater.* 36, 482–488. doi:10.1016/j.optmat.2013.10.014

Wang, S. F., Chen, X. Y., Gao, H. J., Fang, L. M., Hu, Q. W., Sun, G. A., et al. (2021a). A Comparative Study on the Phase Structure, Optical and NIR Reflectivity of BaFe12O19 Nano-Pigments by the Traditional and Modified Polyacrylamide Gel Method. *J. Nano Res.* 67, 1–14. doi:10.4028/www.scientific.net/jnanor.67.1

Wang, S., Gao, H., Fang, L., Hu, Q., Sun, G., Chen, X., et al. (2021b). Synthesis of Novel CQDs/CeO2/SrFe12O19 Magnetic Separation Photocatalysts and Synergic Adsorption-Photocatalytic Degradation Effect for Methylene Blue Dye Removal. *Chem. Eng. J. Adv.* 6, 100089. doi:10.1016/j.ceja.2021.100089

Wang, S., Gao, H., Li, J., Wang, Y., Chen, C., Yu, X., et al. (2021c). Comparative Study of the Photoluminescence Performance and Photocatalytic Activity of CeO2/MgAl2O4 Composite Materials with an N-N Heterojunction Prepared by One-step Synthesis and Two-step Synthesis Methods. *J. Phys. Chem. Sol.* 150, 109891. doi:10.1016/j.jpcs.2020.109891

Wang, S., Gao, H., Yu, H., Li, P., Li, Y., Chen, C., et al. (2020). Optical and Photoluminescence Properties of the MgAl2O4:M (M = Ti, Mn, Co, Ni) Phosphors: Calcination Behavior and Photoluminescence Mechanism. *Trans. Indian Ceram. Soc.* 79, 221–231. doi:10.1080/0371750X.2020.1817789

Wang, S., Tang, S., Gao, H., Chen, X., Liu, H., Yu, C., et al. (2021d). Microstructure, Optical, Photoluminescence Properties and the Intrinsic Mechanism of Photoluminescence and Photocatalysis for the BaTiO3, BaTiO3/TiO2 and BaTiO3/TiO2/CeO2 Smart Composites. *Opt. Mater.* 118, 111273. doi:10.1016/j.optmat.2021.111273

Wang, S., Tang, S., Gao, H., Fang, L., Hu, Q., Sun, G., et al. (2021e). Modified Polyacrylamide Gel Synthesis of CeO2 Nanoparticles by Using Cerium Sulfate as Metal Source and its Optical and Photoluminescence Properties. *J. Mater. Sci. Mater. Electron.* 32, 10820–10834. doi:10.1007/s10854-021-05740-w

Wang, Y., and Tian, H. (2020). Study on the Construction of YMnO3/CeO2 Composite Photocatalyst Heterostructure and Photocatalytic Degradation of Methyl Red. *Optik* 201, 163524. doi:10.1016/j.ijleo.2019.163524

Wen, X.-J., Niu, C.-G., Zhang, L., Liang, C., and Zeng, G.-M. (2018). A Novel Ag2O/CeO2 Heterojunction Photocatalysts for Photocatalytic Degradation of Enrofloxacin: Possible Degradation Pathways, Mineralization Activity and an

in Depth Mechanism Insight. *Appl. Catal. B: Environ.* 221, 701–714. doi:10.1016/j.apcatb.2017.09.060

Xing, S., Song, S., and Xiang, J. (2020). Study on Magnetic, Optical and Photocatalytic Activities of TbMnO3@CeO2 Composite Multiferroic Materials. *Optik* 220, 165144. doi:10.1016/j.ijleo.2020.165144

Conflict of Interest: The authors declare that the research was conducted in the absence of any commercial or financial relationships that could be construed as a potential conflict of interest.

Publisher's Note: All claims expressed in this article are solely those of the authors and do not necessarily represent those of their affiliated organizations, or those of the publisher, the editors and the reviewers. Any product that may be evaluated in this article, or claim that may be made by its manufacturer, is not guaranteed or endorsed by the publisher.